Atmospheric Environment 319 (2024) 120306

Contents lists available at ScienceDirect

Atmospheric Environment

journal homepage: www.elsevier.com/locate/atmosenv

Aerosol-heat flux interactions in the boundary layer during the SIJAQ campaign

Sang-Seok Oh [a], Hyo-Jung Lee [a,b], Min-Seong Kim [a], Moon-Soo Park [c], Cheol-Hee Kim [a,b,*]

[a] Department of Atmospheric Sciences, Pusan National University, Busan, 46241, Republic of Korea
[b] Institute of Environmental Studies, Pusan National University, Busan, 46241, Republic of Korea
[c] Department of Climate and Environment, Sejong University, Seoul, 05006, Republic of Korea

HIGHLIGHTS

- Aerosol-Heat flux-PBL relations are presented during the SIJAQ campaign.
- A sequential process of $PM_{2.5}$–Heat flux–PBL relation was found during the campaign.
- The measured SHF-$PM_{2.5}$ showed strong negative correlation with R of −0.38
- WRF-Chem showed that the aerosol-induced SHF was up to 14% (15 W/m^2).

ARTICLE INFO

Keywords:
Aerosol effects
Sensible heat flux
Latent heat flux
SIJAQ campaign
WRF-Chem modeling

ABSTRACT

The Satellite Integrated Joint Monitoring of Air Quality (SIJAQ) field campaign, carried out from October 10 to November 25, 2021, included the measurement of detailed heat flux and air pollutants. In this study, we interpreted interactions between particulate matter ($PM_{2.5}$) and sensible heat flux (SHF) in the planetary boundary layer (PBL) over the Seoul metropolitan area during the SIJAQ campaign based on measurements and on- and offline WRF-Chem model simulations. Heat flux data obtained during the SIJAQ campaign was varied, depending on meteorological variables, including cloud cover, and revealed meaningful interactions between $PM_{2.5}$ and SHF. Throughout the campaign, the measured $PM_{2.5}$–SHF during the daytime (10:00–16:00 LST) showed overall negative correlation with the correlation coefficient (R) of −0.38. During the campaign, the measured SHF on average was 68 ± 38 W/m^2 on high $PM_{2.5}$ days (daily mean $PM_{2.5} \geq 50$ $\mu g/m^3$), which is significantly lower (35% decrease) compared to the SHF of 105 ± 57 W/m^2 on low $PM_{2.5}$ days (daily mean $PM_{2.5} < 50$ $\mu g/m^3$). Both on- and offline WRF-Chem simulation also showed that SHF and $PM_{2.5}$ were negatively correlated throughout the campaign with R of −0.49, in good agreement with the observations. As the comparative case study, we selected two extreme cases of 3-day periods with the lowest and highest $PM_{2.5}$ concentrations and aerosol effects were estimated based on both on- and offline WRF-Chem simulation and the case-specific aerosol–cloud–SHF–PBL relationship was explored. The results showed that the simulated aerosol-induced SHF was ~14% (15 W/m^2) lower on the highest $PM_{2.5}$ case during the campaign, whereas there was little or no significant relationship on the lowest $PM_{2.5}$ concentration case. Our modeling study also revealed the underlying impact of $PM_{2.5}$ concentrations on reducing SHF (with a slope = −0.41), and this reduction follows a specific sequence of processes: elevated $PM_{2.5}$ level led to a decrease in SHF, weakening the PBL evolution and reducing vertical mixing, ultimately resulting in high $PM_{2.5}$ concentrations accumulated in the PBL over the Seoul metropolitan area.

1. Introduction

Surface heat flux (HF), the sum of sensible heat flux (SHF) and latent heat flux (LHF), have direct impacts on the structure and development of the planetary boundary layer (PBL) (Stull, 1988; Arya, 1988), which acts as a source or sink for energy, and atmospheric pollutants. The PBL plays

* Corresponding author. Department of Atmospheric Sciences, Pusan National University, 2, Busandaehak-ro 63beon-gil, Geumjeong-gu, Busan, 46241, Republic of Korea.

E-mail address: chkim2@pusan.ac.kr (C.-H. Kim).

https://doi.org/10.1016/j.atmosenv.2023.120306
Received 10 July 2023; Received in revised form 11 December 2023; Accepted 13 December 2023
Available online 16 December 2023
1352-2310/

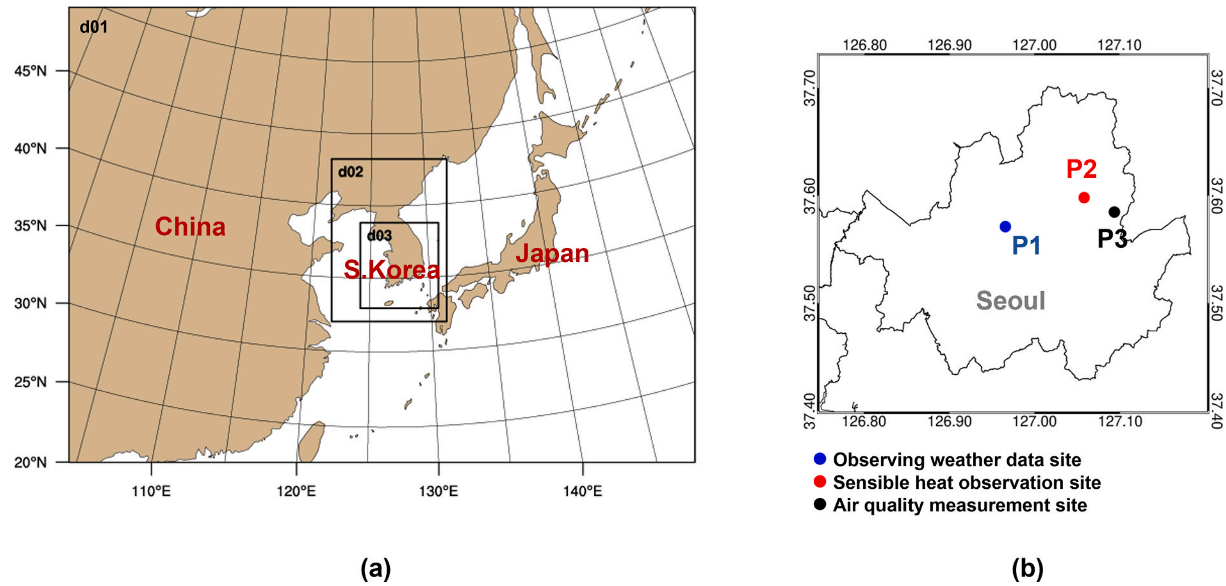

Fig. 1. Weather Research and Forecast (WRF) with chemistry (WRF-Chem) modeling domain (a), and locations of Automated Synoptic Observing System (ASOS) meteorological stations and air-quality-monitoring stations (AQMS) during the Satellite Integrated Joint Monitoring of Air Quality (SIJAQ) campaign over the Seoul metropolitan area (SMA) in South Korea (b). Three nested domains were implemented in the model, covering Northeast Asia (D01; grid spacing, 27 km), the Korean Peninsula (D02; 9 km), and South Korea (D03; 3 km). P1, P2, and P3 indicate weather observation, sensible heat observation, and air quality measurement sites, respectively.

Table 1
Summary of physical and chemical options used in WRF-Chem simulations in this study.

Physics Option	Adopted Scheme
Microphysics	Lin et al. scheme
Longwave radiation	Rapid radiative transfer model (PRTM)
Shortwave radiation	Goddard
Surface layer	Monin-Obukhov similarity
Land surface	Noah Land Surface Model
Planetary boundary layer	Yonsei University scheme (YSU)
Cumulus parameterizations	Grell 3-D
Chemistry Option	**Adopted scheme**
Photolysis	Mandronich photolysis
Gas phase chemistry	NOAA/ESRL RACM Chemistry
Aerosols	Modal Approach Dynamics model for Europe/Volatility Basis Set (MADE/VBS)
Anthropogenic emissions	Comprehensive Regional Emissions inventory for Atmospheric Transport Experiments (CREATEv3 2019)
Biogenic emissions	Model of Emissions of Gases and Aerosols from Nature (MEGAN) v2.04

a significant role in the vertical dispersion of atmospheric pollutants, and surface air pollution levels are heavily influenced by PBL evolution. Thus, HF is a controlling factor of PBL evolution, and its variation has a large impact on the vertical mixing of air pollutants. In this context, detailed HF measurements and analyses are necessary for the determination and prediction of pollution levels throughout the PBL.

Increases in aerosol loading also impact processes within the PBL, because aerosols can alter atmospheric radiative transfer, and subsequent changes in HF directly influence PBL properties. Thus, interactions among aerosols, the PBL, and radiation within the PBL are thought to control the amount of solar radiation reaching the surface. Therefore, aerosols decrease the amount of incident solar radiation, which stabilizes the PBL, and ultimately impedes PBL development, increasing surface aerosol concentrations by feedback. In this context, aerosol–cloud–HF–PBL feedback mechanisms have been studied intensively, including the direct effect of aerosols on flux reduction at global (Liu et al., 2014), regional (Matsui et al., 2008), and *in situ* measurement scales (Murthy et al., 2014). Quan et al. (2014) used field observations of the PBL and *in situ* measurements of air pollutants, and suggested a possible positive feedback between aerosols and PBL during pollution episodes. Petaja et al. (2016) showed that high $PM_{2.5}$ concentrations decreased the amount of solar radiation energy reaching the earth's surface, which led to a reduction in SHF that deteriorated the surface air quality by weakening vertical diffusion processes in the PBL. Liu et al. (2014) showed that SHF had decreased by up to 16 W/m^2 during the period 2003–2010 due to aerosols in the global terrestrial ecosystem, and Matsui et al. (2008) similarly reported decreases of 7.57 W/m^2 in 2000 and 8.36 W/m^2 in 2001 through aerosol–radiation feedback in the eastern USA. In recent years, greater aerosol loading was suggested to effectively reduce incident solar radiation, with cross-regional differences in aerosol–PBL interactions reported in many urban cities in Northeast Asia (i.e., Huang et al., 2023).

Modeling studies have investigated interactions between aerosols and the PBL at various scales. For example, regional-scale simulations have explored aerosol–PBL interactions during periods with high aerosol concentrations using online models (Chen et al., 2015; Sharma et al., 2023). Such models fully couple meteorological and chemical constituents within a single system with two-way interactions, whereas offline models allow only one-way coupling from meteorological to chemical constituents. Previous studies have also shown that the absorption and re-emission of energy by aerosols can result in a smaller temperature difference between the upper and lower atmosphere, leading to a weakened PBL (Miao et al., 2016; Yu et al., 2002). Through such modeling/monitoring studies, aerosol–PBL interactions have been conceptually understood; however, fewer such studies have explored this relationship using actual measured HF mainly due to the paucity of quantitative SHF and LHF measurements and the complexity of aerosol–cloud–HF–PBL interactions.

The Satellite Integrated Joint Monitoring of Air Quality (SIJAQ) field campaign was conducted from October 10 to November 26, 2021. It analyzed the factors contributing to high-particulate matter <2.5 μm in size ($PM_{2.5}$) episodes in the Seoul metropolitan area (SMA). During the campaign, comprehensive measurements of micrometeorological variables, upper air meteorological data, and $PM_{2.5}$ concentrations were concurrently measured over the SMA. This campaign allowed the

Table 2
Cloud cover (%), weather phenomena and insolation(MJ/m^2) at Seoul Station during the SIJAQ campaign. Daytime is defined as the period from 07LST to16LST in this study.

Date (2021)	CC (%)	MLCC (%)	Daytime CC (%)	Daytime MLCC (%)	Daytime LCH (m)	Cloud Type	Insolation (MJ/m^2)	RH (%)	Weather Condition (mm)
18 Oct	66	61	72	61	1522	Sc, As	12.08	60.4	Rain (5.6)
19 Oct	40	40	55	54	730	Sc, St	13.34	72.8	Rain (4.4)
20 Oct	3	3	5	5	1133	Sc	16.7	64.9	–
21 Oct	33	1	53	5	1200	Ci, Sc	5.13	64.1	–
22 Oct	8	3	19	8	1500	Ci, Sc	16.45	58.4	–
23 Oct	3	0	1	0	–	Ci	16.25	57.3	–
24 Oct	3	1	5	1	1000	Ci	15.97	63.1	–
25 Oct	8	3	4	3	1100	Sc, Ci	11.74	64.5	–
26 Oct	36	5	19	0	–	Ci	13.08	74.5	–
27 Oct	25	25	23	23	720	Sc, St	14.72	63.4	Rain (0.0)
28 Oct	0	0	0	0	–		15.58	54.6	–
29 Oct	46	1	42	1	1700	Ci, Sc	14.16	55.9	–
30 Oct	61	40	85	56	1620	Sc, Ci	6.35	62.4	–
31 Oct	38	18	42	15	1060	Ci, Sc	12.25	73.3	Rain (0.7)
1 Nov	30	28	43	43	1120	Sc	11.32	77.3	–
2 Nov	40	14	30	16	977	Sc, Ci	12.69	76.6	–
3 Nov	30	13	9	3	1166	Sc, Ci	13.24	71.1	–
4 Nov	24	21	48	43	1250	Sc	6.9	80.4	Rain (0.0)
5 Nov	6	0	17	0	–	Ci	12.76	68.5	–
6 Nov	13	0	31	0	–	Ci	12.8	61.1	–
7 Nov	70	14	74	3	1000	Ci, Sc	12.2	57.5	–
8 Nov	99	63	100	80	660	St, Ns	2.57	82.1	Rain (25.7)
9 Nov	81	61	99	74	780	St, Ns	3.4	80.3	Rain (2.0)
10 Nov	74	59	81	68	870	Sc, Ac	8.8	73.4	Rain (0.3)
11 Nov	30	30	45	42	1120	Sc	9.68	60.6	Rain (0.0)
12 Nov	13	10	14	14	1000	Sc	13.47	55.4	–
13 Nov	45	45	40	40	1312	Sc	9.9	66.1	–
14 Nov	34	34	32	32	1066	Sc	10.52	69.8	–
15 Nov	36	0	39	0	–	Ci	11.39	81.3	–
16 Nov	0	0	0	0	–		12.07	65.5	–
17 Nov	35	16	28	0	–	Ci	11	64.1	–
18 Nov	75	73	82	82	850	Sc	5.68	70.8	Rain (0.0)
19 Nov	65	49	71	71	710	Sc	4.98	84.8	–
20 Nov	33	10	30	19	850	Sc, Ci	8.62	77.0	–
21 Nov	89	39	97	60	3180	Ac, Cs,	3.3	74.4	Rain (5.9)
22 Nov	33	29	38	38	950	Sc	8.99	61.8	Rain (1.3)
23 Nov	29	29	48	48	1311	Sc	8.4	60.9	–
24 Nov	39	39	53	53	1311	Sc	7.93	64.3	Rain (0.0)
25 Nov	19	19	8	8	1400	Sc	10.25	55.0	–
26 Nov	14	11	37	32	1300	Sc, As	7.6	57.5	Rain (0.0)

CC: Cloud Cover (%).
MLCC: middle and lower cloud cover.
LCH: Lowest cloud height.
Ci: Cirrus, Cs: Cirrostratus, As: Altostratus, Ac: Altocumulus, St: Stratus, Sc: Stratocumulus,
Ns: Nimbostratus.

investigation of relevant $PM_{2.5}$–HF–PBL interactions, and provided an opportunity to perform measurement-based aerosol–cloud–HF–PBL feedback studies over the SMA.

In this study, we explored the relationship between aerosol ($PM_{2.5}$) and HF based on concurrently measured SHF, LHF, PBL, and $PM_{2.5}$ concentrations collected during the SIJAQ campaign. We examined the aerosol–SHF relationship, and then obtained regional modeling results from both on- and offline Weather Research and Forecast (WRF) with chemistry (WRF-Chem) simulations to evaluate and compare aerosol–cloud–HF–PBL interactions and also to estimate the aerosol effects on PBL. As the case study, we selected two 3-day periods with the highest and lowest $PM_{2.5}$ concentrations, and discussed in detail the role of $PM_{2.5}$ in controlling the HF and PBL over SMA.

2. Data and methodology

2.1. Meteorological observations collected during the SIJAQ campaign

During the SIJAQ campaign, various types of micrometeorological variables and pollutants were observed through satellite, aircraft, and *in situ* measurements. SHF and LHF were observed using a surface energy balance system installed at the Hankuk University of Foreign Studies (P2 in Fig. 1). This flux observation system includes sensors that measure basic micrometeorological variables and a sonic anemometer that measures surface SHF and LHF based on a surface energy balance equation; the surface observation system provides 30 min averages of surface HF observations sampled at a frequency of 10 Hz (Park et al., 2017). The process for obtaining surface HF measurements involves physical limit checks, spike detection and removal (Vickers and Mahrt, 1997), 30 min vertical flux averaging (Kwon et al., 2014), and Webb–Peraman–Leuning correction (Leuning, 2007). Quality assurance of the HF measurements was performed as described previously (Kim et al., 2015; Park et al., 2013).

Meteorological observations employed in this study were obtained from at the Automated Synoptic Observing System (ASOS) located in Seoul (126.97°E, 37.57°N; P1 in Fig. 1). Cloud types and cloud cover were measured by a meteorologist's visual evaluation method at Korea Meteorological Administration (KMA), following the 10-category system of the World Meteorological Organization (WMO) (WMO, 1987). Lowest cloud height is also provided by the expert's visual observation conforming to the ground weather observation guidelines of the KMA (KMA, 2022). We utilized daily and daytime average cloud-relevant

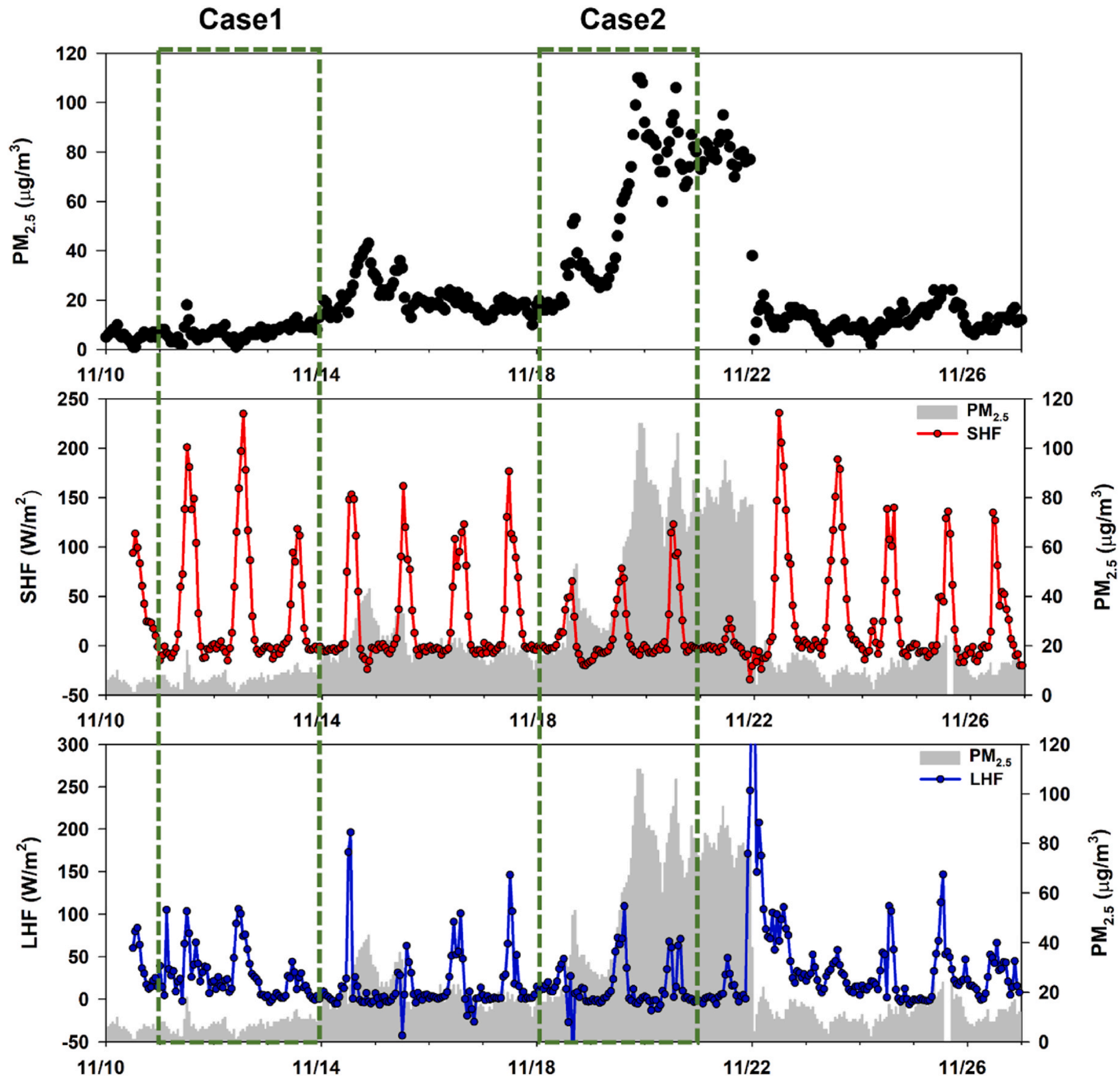

Fig. 2. Time series of sensible heat flux (SHF) and latent heat flux (LHF) observed at site P2 and observed $PM_{2.5}$ concentrations at site P3 from November 10 to 26, 2021, during the SIJAQ campaign. Case 1 and Case 2 denote the periods for two extreme case studies in this study.

variables to consider solar energy at specific times of the day and its impact on accumulated energy affecting SHF. $PM_{2.5}$ concentrations were measured at Jungnang (P3), which is in close proximity (3.4 km apart) to a surface energy balance system site (P2). The Jungnang site is an Air Quality Monitoring Station (AQMS) managed by the Korean Ministry of Environment, which provides concentrations of various pollutants including $PM_{2.5}$, PM_{10}, O_3, NO_2, CO, and SO_2.

2.2. WRF-Chem simulations

To explore the relationships among aerosols, SHF, and LHF, we estimated differences in radiative effects between on- and offline simulations by WRF-Chem. The WRF model was developed by the National Center for Atmospheric Research and includes a chemical transport module (Grell et al., 2005) to consider interactions between meteorological and chemical factors and provide impact pathways for the effects of aerosols on air quality. Sensitivity tests of the on- and offline WRF-Chem modeling results were used to investigate relationships between $PM_{2.5}$ and HF, followed by comparisons of simulated and measured data. Here, the model results that account for the feedback between $PM_{2.5}$ and meteorology are referred to as 'online,' while the results that do not consider this feedback are referred to as 'offline'.

The on- and offline WRF-Chem v3.9.1 models were configured with three nested domains with horizontal resolutions of 27, 9, and 3 km. The horizontal domains are designated D01–D03 and targeted East China, the Korean Peninsula, and South Korea, respectively (Fig. 1). Meteorological initial and boundary conditions were obtained from the National Center for Environmental Prediction (NCEP). The final data had a spatial resolution of $1^\circ \times 1^\circ$ and temporal resolution of 6 h. Grids in the WRF-Chem domain were defined using a Lambert conformal conic projection centered at 38°N, 126°E. All meteorological configurations were identical in the on- and offline WRF-Chem models.

The emissions used for WRF-Chem simulations were the Comprehensive Regional Emissions inventory for Atmospheric Transport Experiments (CREATE) v3 product, which was developed for scientific studies and policy development in East Asia (Woo et al., 2020). The impact of aerosols was quantitatively evaluated using on- and offline WRF-Chem simulations with identical settings, except for the aerosol radiative feedback process, which was independent of meteorological factors and investigated through a comparison of results from two simulations. Taking advantage of the high resolution of the data, we analyzed simulated SHF and LHF over the smallest domain (D03) and

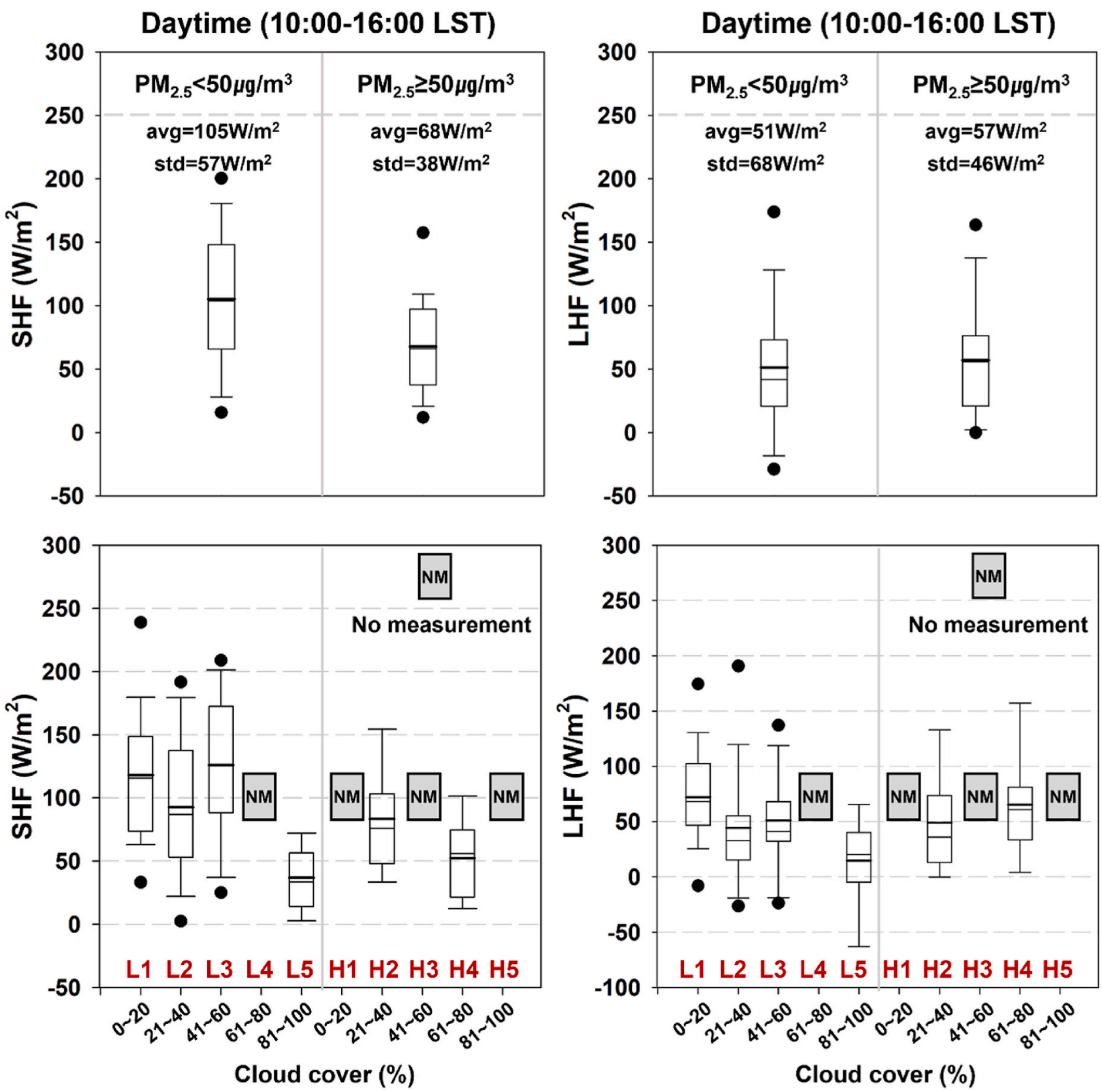

Fig. 3. Box plots of cloud cover and HF (SHF, LHF) versus $PM_{2.5}$ concentrations observed during non-precipitation days. For each box, the center line, boundaries, and dark lines indicate the median, 25th and 75th quartiles, and average values, respectively. Points above and below the box indicate the 5th and 95th percentiles.

compared the simulations with SIJAQ campaign observations. The Model of Emissions of Gases and Aerosols from Nature (MEGAN) v2.04 was used for biogenic emissions. The detailed WRF-Chem options for both meteorology and chemistry are listed in Table 1.

2.3. Evaluation of model performance

To evaluate the meteorological variables simulated by WRF-Chem model, we compared both campaign measurements and ASOS observation data against the model grid values closest to the observation sites. We used statistical indices including the index of agreement ($IOA = 1 - \sum(M_i - O_i)^2 / \sum(|M_i^{'}| - |O_i^{'}|)^2$), Pearson correlation coefficient ($R = [\sum(M_i - \overline{M})(O_i - \overline{O})] / [\sum((O_i - \overline{O})^2)^{1/2} \sum((M_i - \overline{M})^2)^{1/2}]$), and root mean square error ($RMSE = [\sum(M_i - O_i)^2 / N]^{1/2}$) (Kryza et al., 2012; Willmott, 1982) to evaluate the surface temperature at 2 m, wind speed, and HF simulated by the online WRF-Chem model. Here, N is the total sampling number, M_i is the set of model simulations, O_i is the set of observations, $\overline{M}$ is the simulated mean, $\overline{O}$ is the observed mean, and M' and O' represent $M_i - \overline{M}$, and $O_i - \overline{O}$, respectively.

3. Results

3.1. Measurements and simulations of HF and $PM_{2.5}$ during the campaign

The observed solar radiation, cloud covers (%): daily average cloud cover, daytime average cloud cover, middle- and lower cloud cover, and daytime middle- and lower cloud cover, daytime lowest cloud height (LCH), cloud types; Cirrus (Ci), Cirrostratus (Cs), Altostratus (As), Altocumulus (Ac), Stratus (St), Stratocumulus (Sc), Nimbostratus (Ns), insolation, relative humidity, and weather conditions throughout the SIJAQ campaign are summarized in Table 2. From now on, when referred to simply as 'cloud cover' without specific designation, it will be denoted as 'daytime' average cloud cover. From the measurements, inversely proportional relationships were found between daytime average cloud cover and SHF ($R = -0.63$) and LHF ($R = -0.53$). The strong negative correlation between cloud cover and SHF suggests that cloud cover should be classified when examining the aerosol–SHF relationships. Previous studies also mentioned that SHF is greatly influenced by factors such as cloud cover and synoptic meteorological weather conditions in micrometeorological observation analyses (i.e., Stull, 1988).

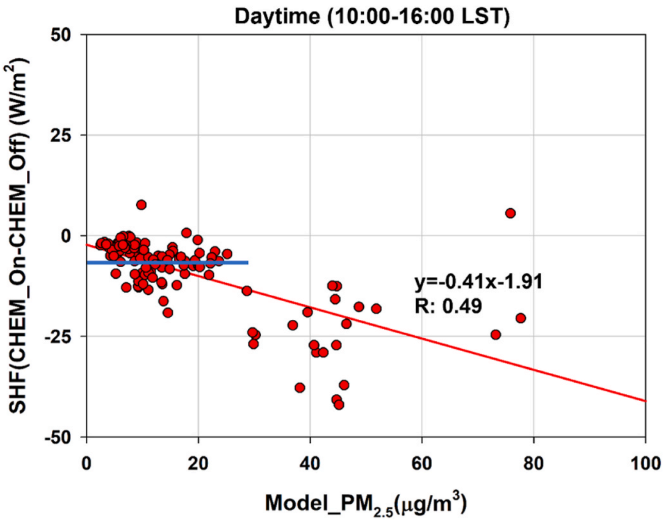

Fig. 4. Scatter diagram of differences between radiative on- and offline SHF modeling results for a range of daytime (10:00–16:00 LST) $PM_{2.5}$ concentrations.

Trends in $PM_{2.5}$, SHF, and LHF observations collected during the SIJAQ campaign are shown in Fig. 2. The period average $PM_{2.5}$ concentration was 24.4 μg/m^3, and the daytime (10:00–16:00 LST) average was 25.2 μg/m^3, with a maximum daily mean of 81.2 μg/m^3 recorded on November 20 (Fig. 2). The highest hourly $PM_{2.5}$ concentration occurred on November 19; it gradually and then rapidly increased in the afternoon of November 19, but still maintained high levels until November 21, with hourly averages of 60–110 μg/m^3. After a precipitation event in the afternoon of November 22, the $PM_{2.5}$ concentration decreased significantly. Micrometeorological variables such as SHF and LHF were measured during the later period of the campaign (November 10–26, 2021); thus, our model results were evaluated for November 10–26, 2021. Throughout the analysis period during the campaign, the average measured SHF was 67.7 ± 38.2 W/m^2 on days with $PM_{2.5} \geq 50$ μg/m^3, while it was 105.0 ± 57.3 W/m^2 on days with $PM_{2.5} < 50$ μg/m^3, clearly indicating significantly lower (35% decrease) in higher $PM_{2.5}$ days (Fig. 3). The measured hourly mean $PM_{2.5}$–SHF for daytime showed strong negative correlation with a correlation (R = −0.38), and there was little correlation between LHF and $PM_{2.5}$ concentrations (R = −0.15).

Cloud effects are playing a role in aerosol–cloud–radiation interactions through the radiation–cloud interactions and chemical reactions, as mentioned many earlier studies (i.e., Park et al., 2018; Lee et al., 2015; Kim et al., 2002). In this study, we classified cloud cover into categories 1–5 (0–20%, 21–40%, 41–60%, 61–80%, and 81–100%, respectively) and $PM_{2.5}$ concentration levels into low and high categories, with $PM_{2.5} < 50$ μg/m^3 designated as L1–L5 and $PM_{2.5} \geq 50$ μg/m^3 as H1–H5. Then we examined the $PM_{2.5}$–HF relationship in detail for the $PM_{2.5}$–cloud cover of 10 subcategories. Variation in SHF and LHF for subcategories L1–L5 and H1–H5 are shown in Fig. 3. Certain combinations of $PM_{2.5}$ concentration and cloud cover contained no HF measurements (i.e., H1, H3, H5, and L4). Overall, SHF levels were higher at low $PM_{2.5}$ concentrations ($PM_{2.5} < 50$ μg/m^3) and lower at high $PM_{2.5}$ concentrations ($PM_{2.5} \geq 50$ μg/m^3). For example, the observed SHF was 92.6 ± 54.7 W/m^2 for L2, but 83.2 ± 39.8 W/m^2 for H2 for the same cloud cover grades, indicating that SHF was ~11% higher at low $PM_{2.5}$ than at high $PM_{2.5}$. However, LHF was 44.3 ± 64.5 W/m^2 for L2 and 48.9 ± 44.4 W/m^2 for H2, with no significant difference between high and low $PM_{2.5}$ conditions. Therefore, we focused on the SHF–$PM_{2.5}$ relationship and aerosol feedback effects on $PM_{2.5}$ concentrations. However, since both cloud and aerosol effects are influenced by synoptic meteorology, it is possible to evaluate the interactions between SHF and $PM_{2.5}$ through on- and offline modeling tests, without the impact of synoptic meteorology contributions.

We conducted on- and offline WRF-Chem simulations for the quantitative analysis of aerosol–SHF interactions during the campaign. Our online models considered aerosol–cloud–radiative effects, whereas our offline models neglected aerosol–cloud–radiation–PBL interactions. The results of both on- and offline WRF-Chem modeling were compared to observation data. The online simulations showed acceptable accuracy for basic meteorological variables such as temperature and wind speed. For temperature, the online WRF-Chem model showed RMSE, IOA, and R values of 1.52, 0.97, and 0.97, comparable to those of the offline simulation (1.56, 0.97, and 0.97, respectively). For wind speed, the online model had RMSE, IOA, and R values of 1.62, 0.72, and 0.69, and the offline model again had comparable values of 1.60, 0.72, and 0.69, respectively. However, the simulation accuracy for SHF was higher in the online simulation, with RMSE, IOA, and R values of 51.85, 0.86, and 0.85, respectively, compared to those of the offline simulation (55.72, 0.85, and 0.85, respectively). Thus, the online simulation performed better than the offline simulation to some extent. These results are consistent with a previous study, which showed that a model including aerosol–radiation interactions performed better than models without aerosol feedback effects (Grell and Baklanov, 2011).

The differences in simulated SHF between the on- and offline WRF-Chem simulations during the campaign and their correlation with $PM_{2.5}$ concentrations were denoted in Fig. 4. As shown in Fig. 4, the simulated differences in SHF were inversely proportional to the $PM_{2.5}$ concentrations with the correlation coefficient (R) of −0.49. The overall trend of SHF had a slope of −0.41, indicating larger negative differences in SHF as $PM_{2.5}$ concentrations increased, whereas there was no

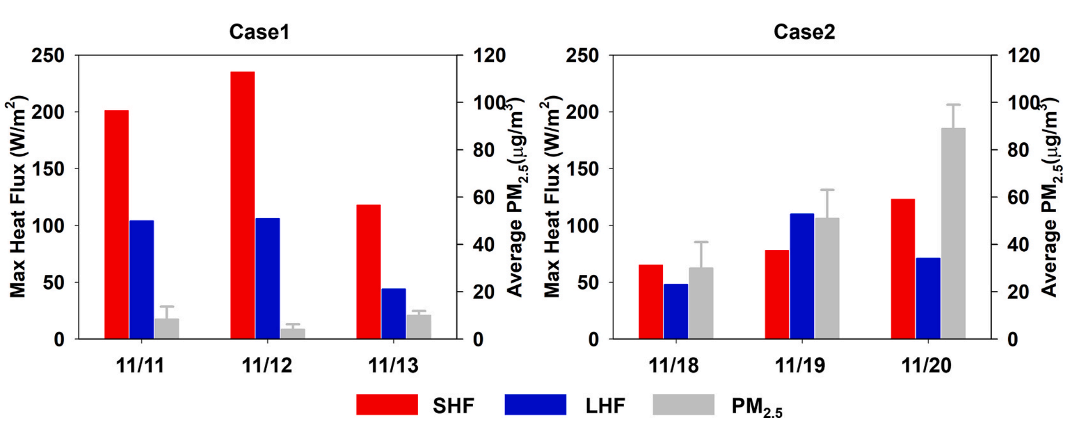

Fig. 5. Maximum SHF and LHF observed at site P2, and daily mean $PM_{2.5}$ observations at site P3 for Case 1 (November 11–13, 2021) and Case 2 (November 18–20, 2021) during the SIJAQ campaign.

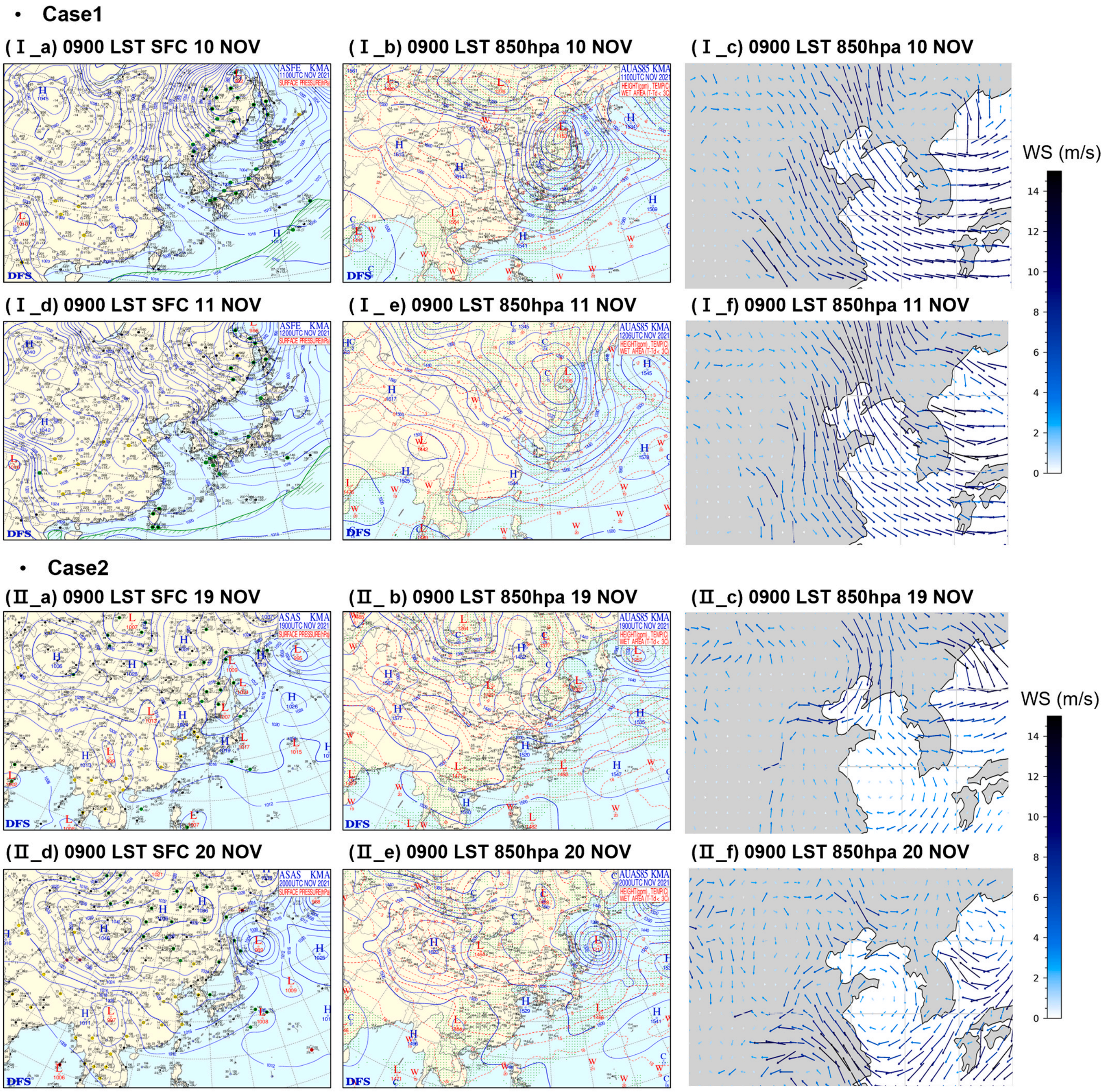

Fig. 6. Surface and 850 hPa weather charts at 0900 LST (0000 UTC), and horizontal wind field distributions at 850 hPa for Case 1 (lowest $PM_{2.5}$ loading period) and Case 2 (highest $PM_{2.5}$ loading period).

significant relationship between the two simulations at lower $PM_{2.5}$ concentrations (i.e., $PM_{2.5} < 20$ μg/m^3). This is again indicating that the sequence of events in the aerosol–SHF relationship and its feedback on $PM_{2.5}$: high $PM_{2.5}$ decreased SHF, which weakened PBL evolution, which led to reduced vertical mixing, resulting in high $PM_{2.5}$ accumulation in the PBL.

3.2. Case studies of aerosol–SHF interactions

As a comparative study, we conducted on and offline simulations for the period with the lowest $PM_{2.5}$ (Case 1; November 11–13) and highest $PM_{2.5}$ (Case 2; November 18–20), and compared two contrasting $PM_{2.5}$ cases to explore the aerosol–SHF relationship in greater detail. Case 1 was the period with the lowest daily $PM_{2.5}$ (November 11–13), and Case 2 had the highest daily $PM_{2.5}$ (November 18–20). For both Case 1 and Case 2, cloud information is available in Table 2, which includes daytime LCH, insolation, and relative humidity, all under similar cloud types, mainly Cs and partially Ci. The most noteworthy differences are observed in the average LCHs, ranging from 1000 to 1312 m for upper-level clouds in Case 1 and 710–850 m for middle-level clouds in Case 2, along with varying insolation, which ranges from 9.7 to 13.5 MJ/m^2 and 5.7–8.6 MJ/m^2, respectively (Table 2).

Daily averages of observed $PM_{2.5}$, SHF, and LHF for both cases are shown in Fig. 5. There were significant differences in observed $PM_{2.5}$ levels between the cases, with daytime average $PM_{2.5}$ concentrations of 7.52 ± 4.13 μg/m^3 for Case 1 (maximum, 18 μg/m^3) and 56.3 ± 27.2

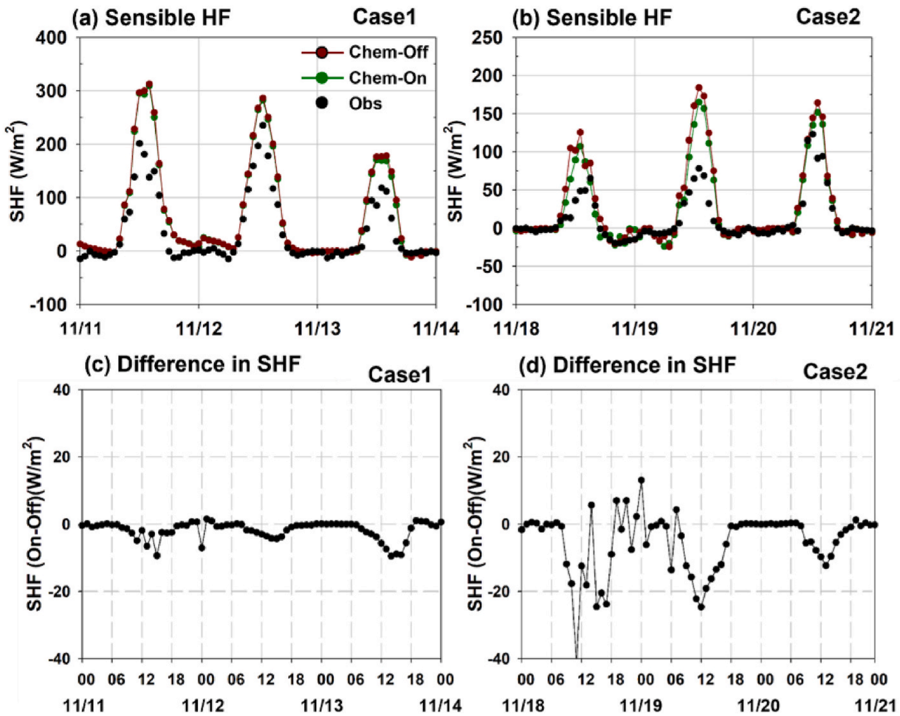

Fig. 7. (a, b) Time series of observed and on- and offline simulated SHF at site P2 for Cases 1 and 2. (c, d) Time series of differences between two model results (on-off).

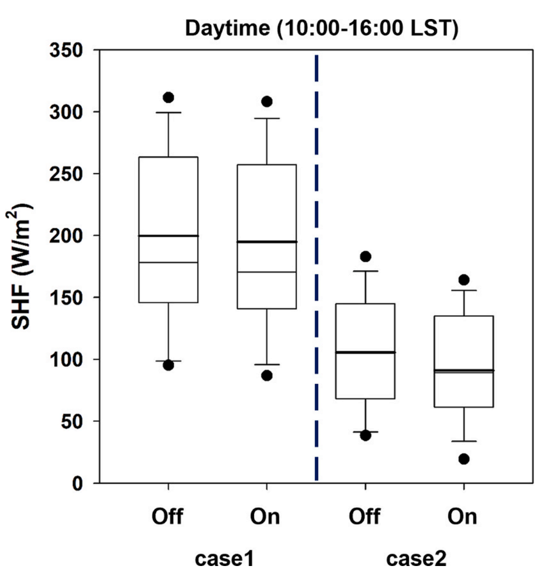

Fig. 8. Box plots of the on- and offline model results of sensible heat flux for Cases 1 and 2 during the daytime (10:00–16:00 LST). For each box, the center line, boundaries, and dark lines indicate the median, 25th and 75th quartiles, and average values, respectively. Points above and below the box indicate the 5th and 95th percentiles.

μg/m^3 for Case 2 (maximum, 106 μg/m^3). The cloud cover ratios for Cases 1 and 2 were (2.9/10) and (5.8/10), respectively; therefore, these cases, characterized by different cloud conditions, were considered suitable for comparatively evaluating the aerosol–SHF relationship in model sensitivity analysis. Observed peak SHF was 185 ± 60.1 W/m^2 for Case 1 (maximum, 235 W/m^2) and 89 ± 30.4 W/m^2 for Case 2 (maximum, 123 W/m^2), indicating significantly lower SHF at high $PM_{2.5}$ concentrations than at low $PM_{2.5}$ concentrations. The daily maximum SHF values for Case 1 were 201, 235, and 118 W/m^2 (November 11–13), mainly exceeding 100 W/m^2 throughout the 3-day period, whereas those for Case 2 were 65, 78, and 123 W/m^2 (November 18–20), with a 52% lower SHF on average on high-$PM_{2.5}$ days than on low-$PM_{2.5}$ days.

In Case 1, the maximum SHF occurred at approximately 12:00 LST, when solar energy was strongest, and approximately 1–2 h later in Case 2 (Fig. 2), suggesting that SHF was perturbed at higher $PM_{2.5}$ levels in Case 2. The SHF peak was sustained for approximately 2 h on November 13 (Case 1), but lasted for only 30 min on November 20 (Case 2) and rapidly declined thereafter. This decrease in SHF in Case 2 may be partly attributed to aerosol effects that decreased incident solar radiation due to high $PM_{2.5}$ levels, which in turn hindered sufficient surface heating. These apparent differences suggest interaction between $PM_{2.5}$ and SHF, which was also discussed in a prior study that highlighted how aerosols impact the scattering and reflection of solar radiation, consequently leading to a reduction in surface SHF in the PBL (Barbaro et al., 2013).

By contrast, no significant differences in LHF were observed between the two cases. The daily maximum LHF values for Case 1 (November 11–13) were 104, 106, and 44 W/m^2, respectively, and those for Case 2 (November 18–20) were 48, 110, and 71 W/m^2, respectively (Fig. 5). In this study, we focused on evaluating the relationship between SHF and $PM_{2.5}$ and related aerosol feedback effects during the campaign in our online modeling tests.

Fig. 6 shows the synoptic conditions obtained from the 1° × 1° NCEP Final product for selected days in each of the two case periods. During November 8–14, 2021 (Case 1), the area was affected by a migratory continental low-pressure system (Kim et al., 2023), and a strong low-pressure system over the northeastern Korean Peninsula, with dense pressure contour lines at both the surface and 850 hPa. As a result, strong winds at 850 hPa (>15 m/s) were observed on November 10, 2021. These were associated with active mixing and resultant lower surface $PM_{2.5}$ levels (Figs. 2 and 5). In Case 2, the synoptic conditions were influenced by a migratory continental high-pressure system. The NCEP Final wind field data indicated slow clockwise patterns over East China, and slow eastward movement of a high-pressure system from the western Korean Peninsula resulted in weakened vertical mixing. Wider spacing between the contour lines of isobars indicated lower wind

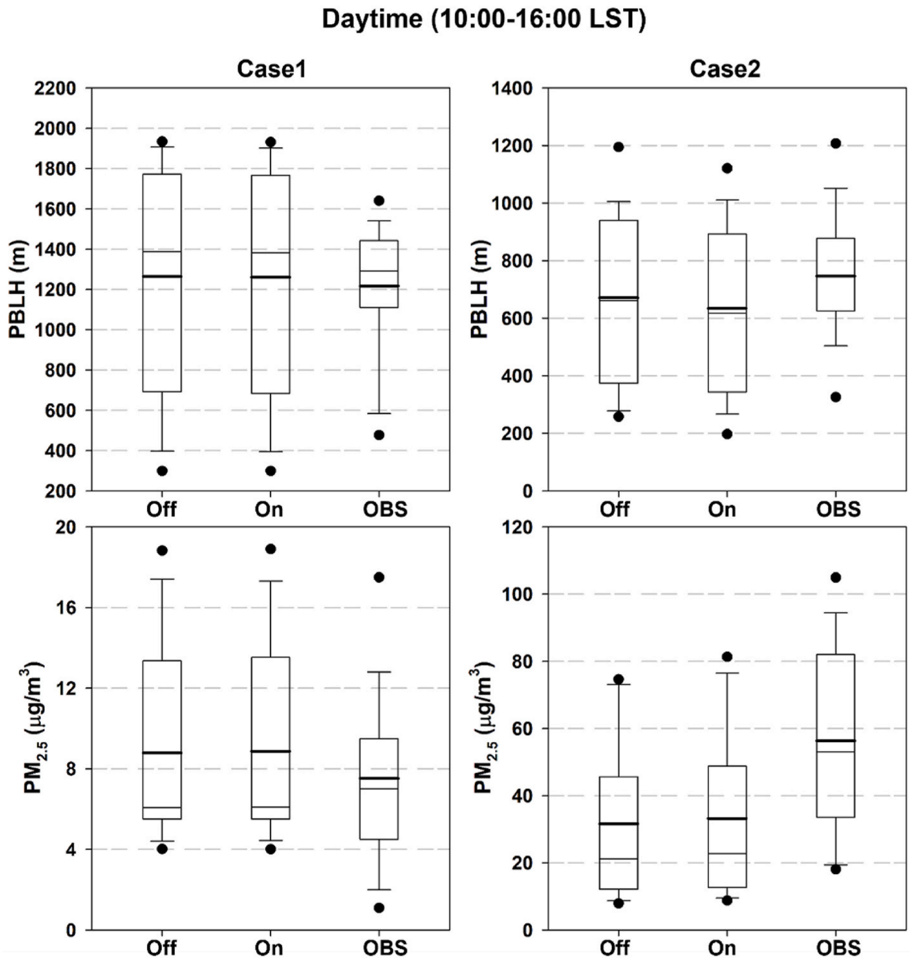

Fig. 9. Box plots of the model results and observation data for Case1 and Case2 during the daytime (10:00–16:00 LST). First row is PBL height (Units: m) and second row is $PM_{2.5}$ concentrations (μg/m^3). The center line in the rectangle, boundaries, dark lines in the box represent the median, 25 and 75 quartiles, and the average value, respectively. The points above and below the box mean 5 and 95 percentiles.

speeds than observed in Case 1. As the high-pressure system moved slowly eastward, pollutants transported by northwesterly winds on November 18 were expected to stagnate above the Korean Peninsula, particularly after November 19. Thus, Case 2 featured low wind speeds under a stagnant pressure high located over the Korean Peninsula, leading to higher surface $PM_{2.5}$ levels due to poor vertical mixing (Figs. 2 and 4), in contrast to the synoptic conditions observed in Case 1. More detailed synoptic descriptions of the campaign period and similar synoptic characteristics during high air quality episodes can be found in previous studies (Kim et al., 2018, 2023).

We used the simulated SHF selected from the smallest high-resolution domain (D03) (Fig. 1); the results for grid points closest to SHF observation site P2 were compared against observations during the campaign. SHF also differed significantly between the cases. At first, we analyzed the simulated cloud microphysical properties which are closely associated with radiative forcing on surface flux, and investigated the response of the $PM_{2.5}$-loaded atmosphere in both the on- and offline models before evaluating the aerosol–SHF relationships.

The differences in simulations on cloud microphysical variables between on- and offline simulations for two cases were illustrated in Fig. S1. As shown, the low, middle, and upper-level cloud fractions in Case 1 were nearly identical between the on- and offline models. However, in Case 2, despite similar cloud cover, some differences were observed. For example, the low-level cloud fraction in Case 2 exhibited some temporal variability; the offline model averaged 46%, while the online model had 44%. Notably, mid-level clouds (clouds at altitudes between 2 and 6 km) had a higher simulated fraction in the offline model at 8%, compared to 2% in the online model (Fig. S1). Shortwave radiation exhibited differences between on- and offline models of up to −15 W/m^2 in Case 1, but online model simulated 45 W/m^2 less peak insolation than offline model in Case 2 (Fig. S1). Cloud water mixing ratios in Case 2 showed relatively higher values from online model, although not significantly different. Further detailed variations in cloud microphysical parameters between the online and offline models in various high $PM_{2.5}$ days can be found in previous studies (i.e., Park et al., 2018; Gao et al., 2020). Differences in other variables including temperature, wind speed, and LHF were found in Fig. S2.

Fig. 7 compares observed and on- and offline simulated SHF for both cases. Despite the overestimation of the peak SHF (November 19) by both the on- and offline simulations, simulated SHF was generally similar between the on- and offline model results for both Cases 1 and 2 (Fig. 7a and b) except for some periods. On November 18, the offline simulation yielded higher overestimations than the online simulation. The online simulation yielded 6% lower average daytime PBL heights and 5% higher $PM_{2.5}$ concentrations than the offline simulation, which overestimated measured SHF and underestimated $PM_{2.5}$ concentrations. This phenomenon is thought to have been caused by reduced vertical mixing due to a SHF decrease caused by aerosol radiative effects. Aerosol perturbations (i.e., offline results–online results) for the two model simulations for both cases are also shown in Fig. 7. SHF perturbations caused by $PM_{2.5}$, particularly during November 18–19, reached −40 W/m^2, which was the maximum difference on hourly basis obtained in this study (Fig. 7c and d).

The daytime average SHF results of the on- and offline models are

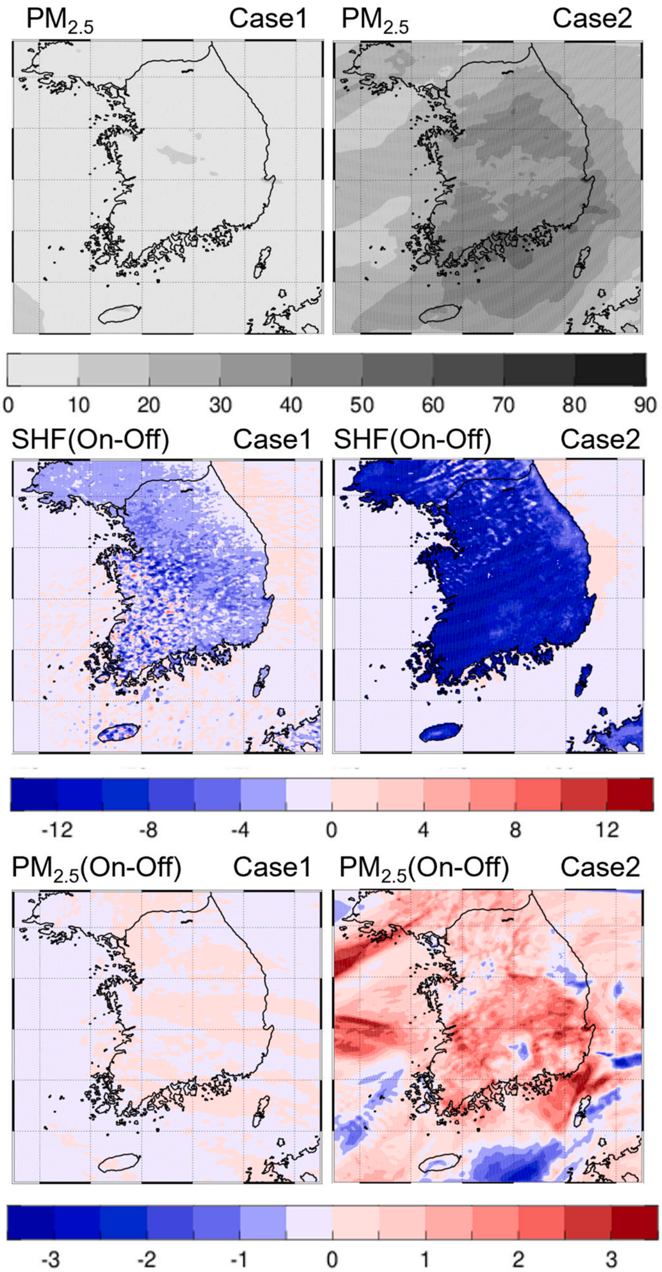

Fig. 10. Horizontal distributions of simulated $PM_{2.5}$ concentrations (μg/m^3) averaged over the daytime (10:00–16:00 LST) (top row), differences in radiative on- and offline WRF-Chem simulations of SHF (W/m^2) (middle row), and differences in $PM_{2.5}$ concentration (bottom row), for Cases 1 and 2.

shown in Fig. 8. In Case 1, simulated SHF did not significantly differ between the models, with 3-day averages of 195 W/m^2 (online) and 200 W/m^2 (offline) with a difference of only −5 W/m^2 which is only 2% lower for Case 1. However, in Case 2, the offline model provided SHF values of 91 W/m^2 (online) and 106 W/m^2 (offline) on daily basis, with a difference of −15 W/m^2. This is believed to be attributed to aerosol–SHF interactions, which were approximately ~14% (15 W/m^2) lower in Case 2.

Fig. 9 provides the comparisons of PBL height and $PM_{2.5}$ concentrations between on- and offline modeling for two specific cases. In Case 1, the daily average $PM_{2.5}$ concentrations, as simulated by both online and offline models, closely approximated 9.3 μg/m^3, in close agreement with the observations. The corresponding PBL heights showed negligible disparities between models, with values of 1.25 and 1.24 km for the on- and offline model, respectively. However, Case 2 exhibited notable differences between models. The online model simulated PBL heights and $PM_{2.5}$ concentrations of 672 m and 31.6 μg/m^3, while the offline model showed 634 m and 33.2 μg/m^3, respectively (Fig. 9). The online model simulated relatively lower PBL heights and considerably higher $PM_{2.5}$ concentrations compared to the offline model. Together, these results indicate lower HF and higher ambient $PM_{2.5}$ concentrations persisting within the PBL during high-$PM_{2.5}$ days (Case 2), when higher $PM_{2.5}$ levels drive the following sequence of events: the aerosol radiative effect reduces incoming surface heating, which reduces HF, weakening the PBL and reducing vertical mixing, which leads to greater $PM_{2.5}$ loading in the PBL. Our results demonstrate the occurrence and extent of aerosol effects on the diurnal evolution of PBL during the SIJAQ campaign due to aerosol–cloud–HF–PBL feedback, based on *in situ* observations and on- and offline meteorology/chemistry simulations. This sequential process was well supported by concurrent HF observations and $PM_{2.5}$ measurements during the SIJAQ campaign.

Fig. 10 shows the horizontal distributions of simulated $PM_{2.5}$ concentration averaged over the daytime (10:00–16:00 LST), and differences in both SHF and $PM_{2.5}$ concentrations between the on- and offline simulations for the two cases. In Case 1, the offline model generally produced higher values, and spatial distributions of differences between the two simulations were within only 5 W/m^2. However, in Case 2, the difference in SHF between the two model simulations was greater at high $PM_{2.5}$ (Fig. 10), and the online SHF simulation was consistently lower, but with domain-average differences >10 W/m^2; this contrasts well with those produced by the offline model. $PM_{2.5}$ concentrations were significantly higher in Case 2 than in Case 1, with notable differences in SHF. This finding is consistent with observations over the SMA, and indicates that the decrease in SHF caused by aerosol reflection and scattering effects reduces vertical mixing, resulting in higher $PM_{2.5}$ concentrations for higher $PM_{2.5}$ loading.

However, long-term observations of aerosol–LHF are needed to sufficiently quantify LHF–$PM_{2.5}$–radiation interactions, particularly for moisture transportation from the Yellow Sea toward the SMA, where there is vigorous secondary formation of $PM_{2.5}$. An analysis of the diurnal variation in secondary and hygroscopic aerosol species composition is also needed to determine how the persistence of these species contributes to high-$PM_{2.5}$ episodes.

4. Summary and conclusions

The SIJAQ field campaign, conducted from October 10 to November 25, 2021, involved the measurement of detailed heat flux. We analyzed aerosol–cloud–HF–PBL interactions based on measurements collected throughout the campaign, and performed on- and offline WRF-Chem simulations to evaluate the impact of $PM_{2.5}$ concentrations on surface SHF. Then, we selected two comparative cases of 3-day periods with the lowest and highest $PM_{2.5}$ concentrations and examined the aerosol–cloud–HF–PBL relationship based on measurements and on- and offline WRF-Chem modeling results, focusing on case-specific $PM_{2.5}$ effects on HF.

HF measurements during the SIJAQ campaign revealed meaningful features of SHF–$PM_{2.5}$ interactions. A clear decrease in SHF was observed, particularly at higher $PM_{2.5}$ concentrations. Throughout the campaign, the measured daytime (10:00–16:00 LST) SHF-$PM_{2.5}$ showed negative correlation with the correlation coefficient (R) of −0.38. The measured SHF on average was 68 W/m^2 on days with $PM_{2.5} \geq 50$ μg/m^3, which is 35% decrease compared to the SHF of 105 W/m^2 on days with $PM_{2.5} < 50$ μg/m^3, indicating the extent of aerosol effects on the diurnal evolution of the PBL due to sequential $PM_{2.5}$–HF–PBL interactions over the SMA.

The on- and offline WRF-Chem simulations also clearly showed an inverse relationship between SHF and $PM_{2.5}$ concentrations (slope = 0.41) throughout the campaign period. In the comparative case study, the simulated SHF on the highest $PM_{2.5}$ case decreased by ~14% (15 W/m^2), whereas surface SHF decreased by ~2% on lowest-$PM_{2.5}$ case. Thus, both observations and simulations of the HF–$PM_{2.5}$ relationship indicated aerosol–HF–PBL interactions over the SMA for the SIJAQ campaign period. Both observational and simulated data clearly suggested a sequential process driven by $PM_{2.5}$ interactions with radiation: a decrease in SHF caused by high $PM_{2.5}$ concentrations weakened PBL evolution, which led to reduced vertical mixing, resulting in high $PM_{2.5}$ accumulations in the PBL. The results of this study will contribute to the improvement of high-$PM_{2.5}$ forecasting accuracy, which is crucial for public health, as well as our understanding of persistent regional haze episodes that occur frequently over the SMA (Jo et al., 2020; Lee et al., 2019).

Although establishing a definitive relationship of aerosol–cloud–SHF–PBL and all the relevant changes in $PM_{2.5}$ concentrations are challenging, there is little doubt that these changes are interconnected. During the SIJAQ campaign, they are also likely to have an impact on, or be clearly influenced by, various aspects of $PM_{2.5}$ concentrations. Therefore, as the next follow-up field campaign to the SIJAQ, it is crucial to conduct a more comprehensive modeling and a well-designed field campaign focused on aerosol–cloud–SHF–PBL feedback process. This comprehensive campaign approach targeting the SMA can provide unveiling the complexity of the feedback process, and understanding the sequential processes of aerosol–HF–PBL for assessing the environmental implications of these changes on urban surface $PM_{2.5}$ concentrations over SMA.

CRediT authorship contribution statement

Sang-Seok Oh: Conceptualization, Data curation, Writing – original draft. **Hyo-Jung Lee:** Conceptualization, Methodology. **Min-Seong Kim:** Data curation, Visualization. **Moon-Soo Park:** Data curation. **Cheol-Hee Kim:** Conceptualization, Funding acquisition, Project administration, Supervision, Validation, Writing – review & editing.

Declaration of competing interest

The authors declare that they have no known competing financial interests or personal relationships that could have appeared to influence the work reported in this paper.

Data availability

Data will be made available on request.

Acknowledgments

This work was supported by a grant from the National Institute of Environmental Research (NIER), funded by the Ministry of Environment (ME) of the Republic of Korea (NIER-2021-04-02-086 and NIER-2022-04-02-037), and also funded by the Basic Science Research Program through the National Research Foundation of Korea (NRF) funded by the Ministry of Education (2020R1I1A2075417 and 2020R1A6A1A03044834).

Appendix A. Supplementary data

Supplementary data to this article can be found online at https://doi.org/10.1016/j.atmosenv.2023.120306.

References

Arya, S.P., 1988. Introduction to Micrometeorology. Academic Press, San Diego.
Barbaro, E., de Arellano, J.V.G., Krol, M.C., Holtslag, A.A.M., 2013. Impacts of aerosol shortwave radiation absorption on the dynamics of an idealized convective atmospheric boundary layer. Bound-Lay Meteorol. 148, 31–49.
Chen, D.S., Ma, X., Xie, X., Wei, P., Wen, W., Xu, T.T., Yang, N., Gao, Q.X., Shi, H.D., Guo, X.R., Li, Y., Zhou, Y., Lang, J.L., 2015. Modelling the effect of aerosol feedbacks on the regional meteorology factors over China. Aerosol. Air Qual. Res. 15, 1559–1579.
Gao, M., Han, Z.W., Tao, Z.N., Li, J.W., Kang, J.E., Huang, K., Dong, X.Y., Zhuang, B.L., Li, S., Ge, B.Z., Wu, Q.Z., Lee, H.J., Kim, C.H., Fu, J.S., Wang, T.J., Chin, M., Li, M., Woo, J.H., Zhang, Q., Cheng, Y.F., Wang, Z.F., Carmichael, G.R., 2020. Air quality and climate change, Topic 3 of the Model Inter-Comparison Study for Asia Phase III (MICS-Asia III) - Part 2: aerosol radiative effects and aerosol feedbacks. Atmos. Chem. Phys. 20, 1147–1161.
Grell, G., Baklanov, A., 2011. Integrated modeling for forecasting weather and air quality: a call for fully coupled approaches. Atmos. Environ. 45, 6845–6851.
Grell, G.A., Peckham, S.E., Schmitz, R., McKeen, S.A., Frost, G., Skamarock, W.C., Eder, B., 2005. Fully coupled "online" chemistry within the WRF model. Atmos. Environ. 39, 6957–6975.
Huang, X., Wang, Y.Y., Shang, Y., Song, X.R., Zhang, R., Wang, Y.X., Li, Z.Q., Yang, Y.J., 2023. Contrasting the effect of aerosol properties on the planetary boundary layer height in Beijing and Nanjing. Atmos. Environ. 308.
Jo, Y.-J., Lee, H.-J., Jo, H.-Y., Woo, J.-H., Kim, Y., Lee, T., Heo, G., Park, S.-M., Jung, D., Park, J., Kim, C.-H., 2020. Changes in inorganic aerosol compositions over the Yellow Sea area from impact of Chinese emissions mitigation. Atmos. Res. 240.
Kim, C.-H., Jo, H.-Y., Jo, Y.-J., Lee, H.-J., Kim, J.-M., Lee, N.-M., Jeong, S.-Y., Baek, S.-H., Park, M.-J., Chang, L.-S., Lee, J.-J., Song, C.-K., 2023. Synoptic meteorological conditions and contributing factors to air quality during the SIJAQ campaign. Atmos. Environ. 309.
Kim, C.-H., Kreidenweis, S.M., Feingold, G., Frost, G.J., Trainer, M.K., 2002. Modeling cloud effects on hydrogen peroxide and methylhydroperoxide in the marine atmosphere. J. Geophys. Res. Atmos. 107.
Kim, C.-H., Lee, H.-J., Kang, J.-E., Jo, H.-Y., Park, S.-Y., Jo, Y.-J., Lee, J.-J., Yang, G.-H., 2018. Meteorological overview and signatures of long-range transport processes during the MAPS-Seoul 2015 campaign. Aerosol Air Qual. Res. 18, 2173–2184.
Kim, W., Miyata, A., Ashraf, A., Maruyama, A., Chidthaisong, A., Jaikaeo, C., Komori, D., Ikoma, E., Sakurai, G., Seoh, H.H., Son, I.C., Cho, J., Kim, J., Ono, K., Nusit, K., Moon, K.H., Mano, M., Yokozawa, M., Baten, M.A., Sanwangsri, M., Toda, M., Chaun, N., Polsan, P., Yonemura, S., Kim, S.D., Miyazaki, S., Kanae, S., Phonkasi, S., Kammales, S., Takimoto, T., Nakai, T., Iizumi, T., Surapipith, V., Sonklin, W., Lee, Y., Inoue, Y., Kim, Y., Oki, T., 2015. FluxPro as a realtime monitoring and surveilling system for eddy covariance flux measurement. J. Agric. Meteorol. 71, 32–50.
Korea Meteorological Administration (KMA), 2022. Guidance of Surface Meteorological Observation. Seoul, Korea. (in Korean).
Kryza, M., Werner, M., Dore, A.J., Vieno, M., Blas, M., Drzeniecka-Osiadacz, A., Netzel, P., 2012. Modelling meteorological conditions for the episode (December 2009) of measured high PM10 air concentrations in SW Poland - application of the WRF model. Int. J. Environ. Pollut. 50, 41–52.
Kwon, T.H., Park, M.-S., Lee, C.Y., Choi, Y.J., 2014. Effects of different averaging operators on the urban turbulent fluxes. Kor. Meteorol. Soc. 24, 197–206.
Lee, H.J., Jo, H.Y., Park, S.Y., Jo, Y.J., Jeon, W., Ahn, J.Y., Kim, C.H., 2019. A case study of the transport/transformation of air pollutants over the Yellow Sea during the MAPS 2015 campaign. J. Geophys. Res. Atmos. 124, 6532–6553.
Lee, H.J., Kang, J.E., Kim, C.H., 2015. Forty-year (1971-2010) semiquantitative observations visibility-cloud-precipitation in Korea and its implication for aerosol effects on regional climate. J. Air Waste Manag. Assoc. 65 (7), 788–799.
Leuning, R., 2007. The correct form of the Webb, Pearman and Leuning equation for eddy fluxes of trace gases in steady and non-steady state, horizontally homogeneous flows. Bound-Lay Meteorol 123, 263–267.
Liu, S.Q., Chen, M., Zhuang, Q.L., 2014. Aerosol effects on global land surface energy fluxes during 2003-2010. Geophys. Res. Lett. 41, 7875–7881.
Matsui, T., Beltran-Przekurat, A., Niyogi, D., Pielke, R.A., Coughenour, M., 2008. Aerosol light scattering effect on terrestrial plant productivity and energy fluxes over the eastern United States. J. Geophys. Res. Atmos. 113.
Miao, Y.C., Liu, S.H., Zheng, Y.J., Wang, S., 2016. Modeling the feedback between aerosol and boundary layer processes: a case study in Beijing, China. Environ. Sci. Pollut. Res. 23, 3342–3357.
Murthy, B.S., Latha, R., Kumar, M., Mahanti, N.C., 2014. Effect of aerosols on evapotranspiration. Atmos. Environ. 89, 109–118.
Park, M.S., Joo, S.J., Lee, C.S., 2013. Effects of an urban park and residential area on the atmospheric CO2 concentration and flux in Seoul, Korea. Adv. Atmos. Sci. 30, 503–514.
Park, M.S., Park, S.H., Chae, J.H., Choi, M.H., Song, Y., Kang, M., Roh, J.W., 2017. High-resolution urban observation network for user-specific meteorological information service in the Seoul Metropolitan Area, South Korea. Atmos. Meas. Tech. 10, 1575–1594.
Park, S.-Y., Lee, H.J., Kang, J.E., Lee, T.Y., Kim, C.H., 2018. Aerosol radiative effects on mesoscale cloud-precipitation variables over Northeast Asia during the MAPS-Seoul 2015 campaign. Atmos. Environ. 172, 109–123.

Petaja, T., Jarvi, L., Kerminen, V.M., Ding, A.J., Sun, J.N., Nie, W., Kujansuu, J., Virkkula, A., Yang, X.Q., Fu, C.B., Zilitinkevich, S., Kulmala, M., 2016. Enhanced air pollution via aerosol-boundary layer feedback in China. Sci Rep-Uk 6.
Quan, J.N., Tie, X.X., Zhang, Q., Liu, Q., Liu, X., Gao, Y., Zhao, D.L., 2014. Characteristics of heavy aerosol pollution during the 2012-2013 winter in Beijing, China. Atmos. Environ. 88, 83–89.
Sharma, A., Venkataraman, C., Muduchuru, K., Singh, V., Kesarkar, A., Ghosh, S., Dey, S., 2023. Aerosol radiative feedback enhances particulate pollution over India: a process understanding. Atmos. Environ. 298.
Stull, R.B., 1988. An Introduction to Boundary Layer Meteorology. Springer Netherlands, Dordrecht.
Vickers, D., Mahrt, L., 1997. Quality control and flux sampling problems for tower and aircraft data. J. Atmos. Ocean. Technol. 14, 512–526.
Willmott, C.J., 1982. Some comments on the evaluation of model performance. Bull. Am. Meteorol. Soc. 63, 1309–1313.
Woo, J.H., Kim, Y., Kim, H.K., Choi, K.C., Eum, J.H., Lee, J.B., Lim, J.H., Kim, J., Seong, M., 2020. Development of the CREATE inventory in support of integrated climate and air quality modeling for Asia. Sustainability-Basel 12.
World Meteorological Organization (WMO), 1987. International Cloud Atlas, vol. II. WMO No. 407, Geneva, Switzerland.
Yu, H.B., Liu, S.C., Dickinson, R.E., 2002. Radiative effects of aerosols on the evolution of the atmospheric boundary layer. J. Geophys. Res. Atmos. 107.